JLCX-002
Aug. 2002

JLC X-BAND TECHNICAL NOTE

Characteristics of RF-QC and the measurement results on RDDS1 disks

T. Higo*, N. Toge*, G. Bowden$, J.W. Wang$, R. H. Miller$, Z. Li$

* KEK, High Energy Accelerator Research Organization
1-1, Oho, Tsukuba, Ibaraki, 305-0801, Japan

$ SLAC, Stanford Accelerator Center, Stanford university
Sand Hill Rd., Menlo Park, CA, 94305, UAS

Abstract

The RF performance of RDDS1 disks was evaluated soon after machining. The disk-to-disk scatterings of higher-order modes in addition to the modes representing the accelerating mode were evaluated. The absolute frequency of the accelerating mode of six consecutive disks was measured and feed-forwarded to the inner diameter parameters for the following disk fabrication to keep the integrated phase error of accelerating mode within 5 degrees over the whole structure.

Characteristics of RF-QC and the measurement results on RDDS1 disks

T. Higo*, N. Toge*, G. Bowden$, J.W. Wang$, R. H. Miller$, Z. Li$

* KEK, High Energy Accelerator Research Organization
1-1, Oho, Tsukuba, Ibaraki, 305-0801, Japan

$ SLAC, Stanford Accelerator Center, Stanford university
Sand Hill Rd., Menlo Park, CA, 94305, UAS

Abstract

The RF performance of RDDS1 disks was evaluated soon after machining. The disk-to-disk scatterings of higher-order modes in addition to the modes representing the accelerating mode were evaluated. The absolute frequency of the accelerating mode of six consecutive disks was measured and feed-forwarded to the inner diameter parameters for the following disk fabrication to keep the integrated phase error of accelerating mode within 5 degrees over the whole structure.

1. Introduction

We have been designing X-band travelling-wave structures which serve for the acceleration of the beam over a long distance with preserving its low emittance by applying detuning of higher order modes in addition to medium damping of the modes[1,2]. In order to make the detuning effective, the frequencies of the lowest dipole modes should be controlled within 3 MHz in sigma. The frequency of the accelerating mode should also be tuned well to make the acceleration effective. We set a criteria on this such that the integrated phase advance along the structure does not exceed 5 degrees.

Over than several years, we have fabricated detuned structures[1,3] and damped-detuned structures[1,2] aiming at the linear collider purpose. The 2D shape of the constituent cells of these structure can be described as a cylinder with a thin wall (disk) at one of the end of the cylinder. The fabrication of these cells are described in references [4]. The fabricated cells are electrically checked cell by cell set on a floating choke set up. The most sensitive dimension “2b”, the cell inner diameter, is checked by exciting a cell in a pseudo-accelerating mode[1].

Recently we designed a structure called “rounded damped detuned structure”, RDDS[5,6,7,8]. The main different feature of this design is the rounding of the cell inner shape to make the shunt impedance higher. Due to this shape, it is natural to divide the structure to its constituent part, called “disk’, which comprises of a disk with a beam hole at the middle of the disk while the accelerating cell is divided into

half to be attached at both side of the middle disk. Due to this change, we changed the set up for the electrical checking of the disks after machining.

In the present paper, we describe how we designed the measurement and how it behaves for the RDDS1 disk evaluation. The measurement includes the evaluation of the disk scattering from a smooth curve in addition to the absolute measurement of the accelerating mode in every six disks.

Based on the measurement, we made some feed forward process in the fabrication of the later disks. The result of this approach is also reviewed.

2. General design of frequency measurement

2-1 Disk-to-disk smoothness

The schematic shape of the RDDS1 disk is shown in Fig. 2.1(a). As shown in the figure, the disk is symmetric with respect to its middle plane. Therefore, if we close both sides of the disks with flat conducting planes, we can easily measure 0 and π mode shown with solid circles in Fig. 2.1(b). It is possible to estimate the scattering of accelerating mode frequency from the two frequencies of the monopole modes. The lowest dipole mode which is synchronous to the beam is near π mode and this π mode can be measured directly in the same set up. The only action needed is to place the antenna off axis. The 0 mode of the dipole mode usually represents the 0-mode of the second dipole pass band. These four modes are to be measured in every single-disk set up to evaluate the smoothness of the frequencies from disk to disk.

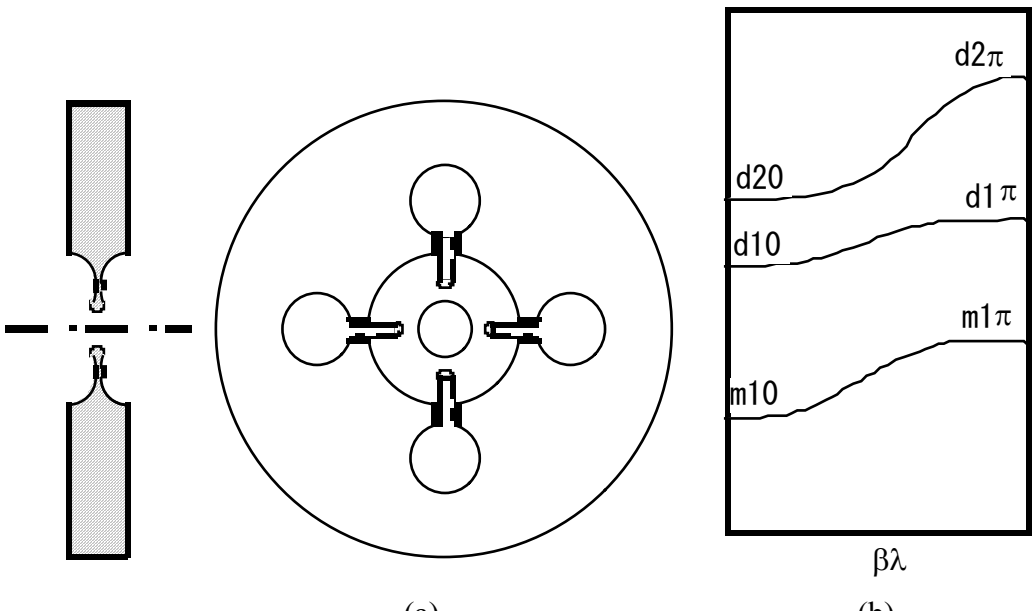

Fig. 2.1 (a) Schematic shape of RDDS disk and (b) zero and π mode of three dispersion curves.

2-2 Absolute accelerating-mode frequency

The accelerating mode frequency should be evaluated as the absolute value. Following are a few concerns to realize the measurement.

Boundary condition

Even if the dimensions vary as functions of disk number along a structure, the parameters should realize 2π/3 mode in every cell. Because each disks is designed to be cut at the center of each cell, we can establish a 2π/3 standing wave by making a set up with a stack of a multiple of three disks. The standing wave field in a three-cell set up is connected to the nest three-cell set up to form a standing wave in a six-cell set up. Here, the frequency perturbation by the probes in three-disk set up is twice of that in a six-disk set up. Therefore, we can obtain the frequency free from the probe perturbation by the equation

$$F_\infty = F_6 + (F_6 - \frac{F_{3L} + F_{3R}}{2}),$$

where F_∞, F_6, F_{3L} and F_{3R} are the frequencies of 2π/3 mode in a periodic boundary condition, that measured in a six-disks set up and those measured in three-disk set up comprising of left and right three disks in a six-disk set up. The frequency thus obtained should be noted as the average frequencies of six independent disks.

Contact pressure

The effect due to the unstable mechanical geometry is confirmed to be negligible if the electrical properties are saturated as for the application of the contact pressure. The practical situation is described in the following chapter.

Skin depth

If we want to estimate the frequency with a better precision than the effect due to finite skin depth, F/2Q, this effect should be included to compare with the theoretically obtained frequency where infinite conductance is assumed. The Q value can be cited from the calculated one. In the present case, simple Q=7000?? was assumed.

Frequency correction to nominal environments

The structure is to be operated in vacuum at a temperature of 45 ºC. The measured frequencies should be converted to this nominal environment. The test set up is usually filled with nitrogen gas and kept in a temperature controlled clean room until the temperature of the disk is stabilized.

The volume where the RF field exists is filled with nitrogen gas. The flow rate is typically fixed at 0.2cc/min. The measured frequency was found not sensitive to the flow rate. If the atmospheric pressure changes by a few %, the dielectric constant of the gas changes proportionally and the resultant frequency change is about 0.1MHz. We ignored this correction this time. We did not have any great typhoon during RDDS1 measurement.

The humidity of air is also a possible source of dielectric constant if the air fills the volume. In the present case, the gas is principally replaced by nitrogen gas and the effect from air humidity can be ignored. The water layer absorbed on the surface of disk before set up can be possible source of frequency error. We made a series of

frequency measurements after onset of the nitrogen purge for a few minutes to make sure the change of frequency is small.

Finally, we chose the thermal expansion coefficient for copper based on the nominal number which SLAC uses. Then we took the following correction formula,

$$F_{operation} = F_{measurement} \times \{1 + \alpha \times (T - 45) + \frac{\varepsilon - 1}{2} \times \frac{20 + 273}{T + 273})\},$$

where

$\alpha = 1.68 \times 10^{-5}$ (thermal expansion coefficient),

$\varepsilon = 1.000547$ (dielectric constant of nirogen gas) and

T = temperature in degree centigrade.

3. Characteristics of experimental set up

3.1 Experimental set up

Fig. 3.1 shows the schematic view of the 6-disk set up. The set up is located in a clean room of class 10000. The set up is made on a board located 1m above flore level and right under an HEPA filter on the ceiling at 2.3m high. The temperature of the outlet from the filter is typically controlled at 23+-0.2 ºC.

The disks under test are stacked on a V-block. These disks are sandwiched by two cylindrical end plates. Each end plate is backed by two stainless-steel plates. Each plate is pressed independently by a fine-pitch screw boosted by a factor 9 using an oil pumping mechanism. Two strain gauges are inserted to measure the pressure independently.

End plate is equipped with two thin holes, one for inserting a semi-rigid cable to form an antenna at 4mm offset from axis and the other as an inlet or an outlet of nitrogen gas located facing the HOM manifold. These holes are located roughly upward direction.

The rotational angle of disks are aligned using alignment notch with respect to the V-block such that the manifolds are located either horizontal or vertical position. Since the probe angle is also fixed with respect to the V-block, the probes are facing at the angle of one of the manifolds.

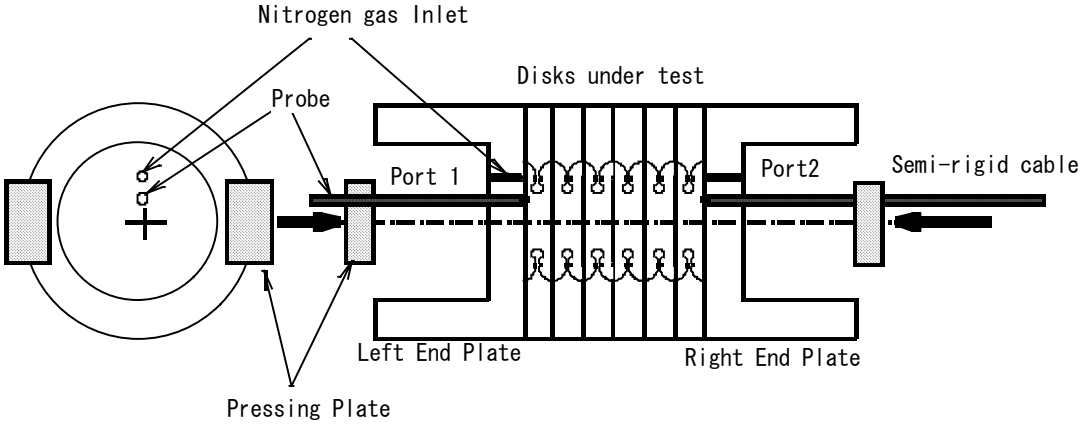

Fig. 3.1 Schematic drawing of stacked-disk QC set up.

3.2 Stabilization of disk temperature

The clean room temperature is controlled at 21℃ but the temperature of human being is about 30℃ so that there is a difference between them about 10℃. Therefore, if we handle disks by hand, we need to wait for a while before the RF measurement. Fig. 3.2 shows a history of the temperature of a disk through various handling processes. As seen in the figure and the similar tests, we found the rate of temperature change and the convergence to the equilibrium value as listed in Table 3.1.

The temperature changing rates in various handling processes are listed in Table where the temperature difference between the disk and hand is about ten degrees.

What we conclude from the above study is that in a stacked-disk measurement, the disk under test can be temperature equalized very quickly.

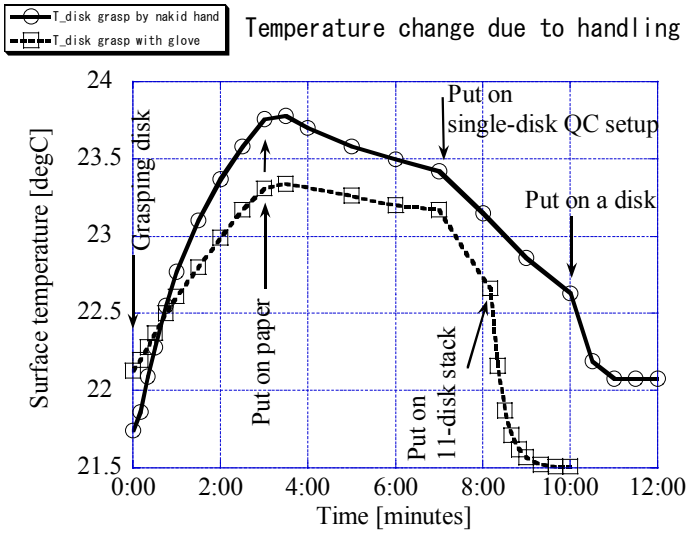

Fig. 3.2 Temperature drifts due to various handling processes. Open circles are the temperatures starting by grasping a disk with naked hand while those with open squares are those started by grasping with glove.

Table 3.1 Rate of disk temperature change due to various handling processes.

Handling process	dT/dt [℃/min]	ΔT [℃]
Grasp by naked fingers	1	10
Grasp with glove	0.5	10
Put on a paper	0.05 to 0.2*	2
Put on a paper	1.4	9
Put on a metal plate	25	8
Put on single-disk floating set up	0.1%	1
Put on 11-disk stack	3#	1
Put on a disk	>1$	1

* Saturate after initial change of about 0.5℃ even if there remians more than 1.5℃ temperature difference.

% Sitting on three thin teflon rods for floating single-disk QC setup.

It is to be noted that the temperature reached within 0.1℃ to that of the 11-disk stack in one minute.

$ Reaches to the average value of the temperatures of two disks in a minute.

3.3 Contact pressure

The dependence of frequency and Q value on contact pressure was measured as shown in Figs. 3.3 and 3.4. From these examples, we can conclude that the frequency error is less than 0.1MHz if we apply more than 50kg over the surface. On the other hand, the Q value cannot be fully saturated even 300kg. We decided to apply 400kg for the RDDS1 measurement to make the measurement in a better behaved resonant curve where the pressure is well beyond the frequency saturation.

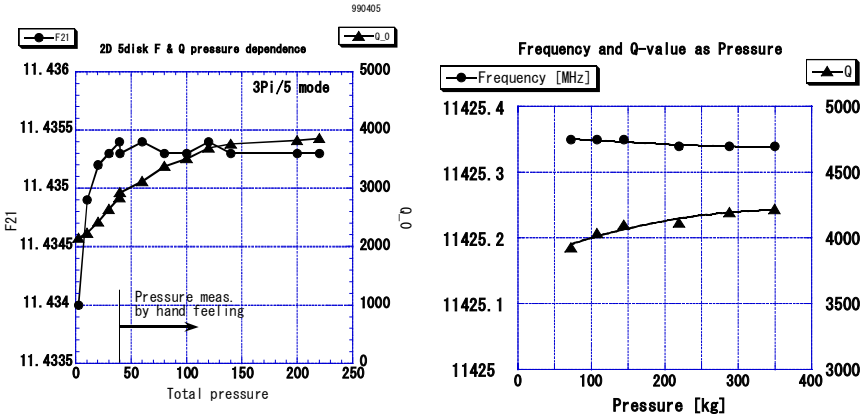

Fig. 3.3 Frequency and Q value of 3π/5 and 2π/3 mode in 5-disk and 6-disk stack set up as function of compressing force.

3.4 Dependence on probe length

The smaller the perturbation due to probe, the more stable becomes the absolute frequency measurement if the coupling of the probe to the mode is large enough. One of the most significant dimensions in this respect is the intrusion of the antenna. The antenna intrusion is the difference of the inner conductor height, probe length, and the thickness between the base of the semi-rigid cable to the cavity surface, which is about 3.00mm.

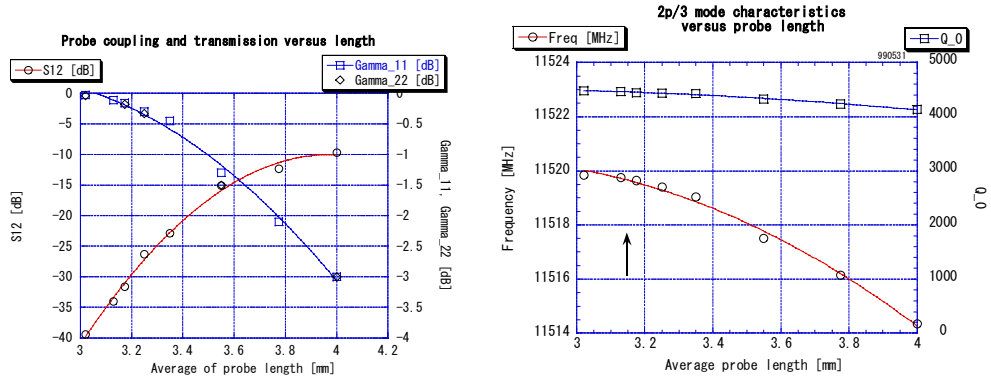

(a) (b)

Fig. 3.4 (a) Transmission and reflection as function of probe length. (b) Measured frequency and Q value as function of probe length. Actual length cited for the measurement is shown as arrow.

Fig. 3.4(a) shows the amplitude of the transmission between two probes as a function of probe length and the reflection coefficient of each probe. Since the noise level is much less than -40dB?, it is reasonable to choose around 3.2mm for the probe

length by considering the possibility to measure the multi-disk stack with over than 40 disks where the transmission is reduced by 10 dB or more.

Actual probe length was chosen to be 3.17mm, which corresponds to the intrusion of the antenna inner conductor by 0.17mm. As seen from Fig. 3.4(b) the frequency perturbation in this case is about one third of MHz, which makes the error in the corrected frequency much less than 0.1MHz. In this parameter, the coupling of the probe is only 0.02, resulting in a Q value degradation only by 4% or so.

3.5 Probe position and hole size

The hole for the antenna to be inserted should be as small as possible to make the perturbation minimum but there should have a gap to the center conductor of the semi-rigid cable with its diameter of 0.5mm. The hole diameter was set at 1.00± 0.01mm.

In order to measure dipole modes in addition to monopole modes, the probe should be located offset from the axis. The frequency perturbation and coupling of the probe depends on the amount of the offset. Fig. 3.5 shows the field profile along the radial line on the end surface for the representative disks, one at front end and another at the output end. General trend of the field profile is the same over the full length of the structure. If we apply the Slater's perturbation formula using these calculated fields, the frequency perturbation due to the hole is calculated as shown in Fig. 3.6(a). We found that the best position to minimize the perturbation of the probe is around r=7mm.

Though the minimum sensitivity is realized at r=7mm, we already?? chose r=4mm based on a rough estimate based on a pillbox approximation. Due to time limitation, we did not redesign to make the perturbation minimum. We measured all the RDDS1 disks with r=4mm set up.

Fig. 3.6(b) indicates that the frequency perturbation due to probes and holes increases from the front side to the output side in we choose r=4mm. The electric field plays an important role for this dependence. In future design, we had better choose the position around r=7mm.

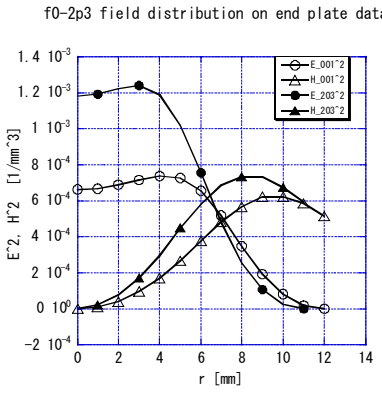

Fig. 3.5 Calculated field profile of accelerating mode along radial position on the end surface.

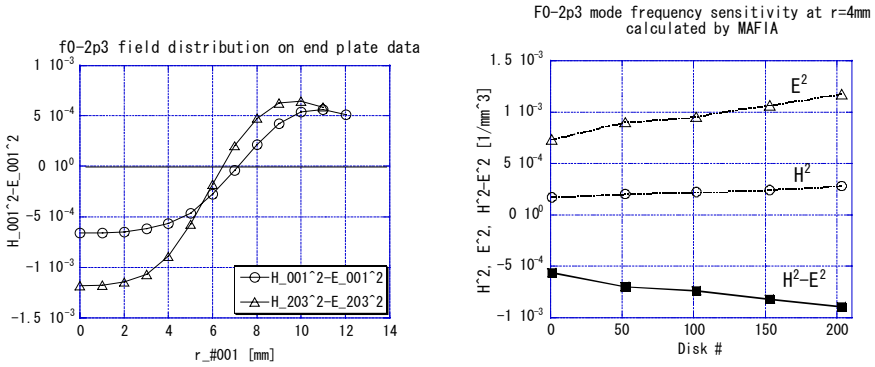

(a) (b)

Fig. 3.6 (a) Calculated frequency perturbation versus radial position.
(b) Perturbation of probes and holes as function of disk numbering.

3.6 Dependence on number of stacked disks

The amplitude of transmission measurement between two probes located at two ends was measured as function of number of stacked disks. The result in Fig. 3.7 shows the transmission power scaled as $N^{-1.6}$ where N is the number of stacked disks. From this figure, it is to be noted that if we want to use the same probes to measure the stack with such as 39 disks as we did before to evaluate the absolute frequency with little error due to the direct probe perturbation, it is necessary to tune the coupling of the probe about 20dB above noise level.

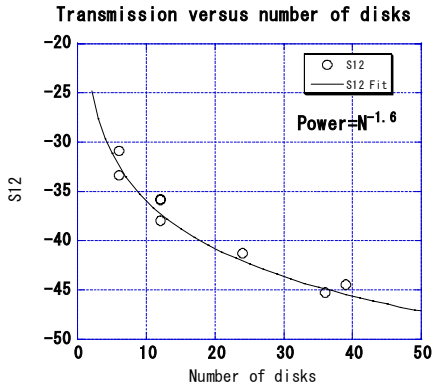

Fig. 3.7 Magnitude of transmission versus number of stacked disks.

4. RF QC results

4.1 Single-disk RF QC

Frequencies of the lowest four modes excited in a single disk sandwiched by two flat plates each equipped with an antenna at offset by 4 mm from the mechanical axis. The measured frequencies are plotted as functions of design synchronous frequency of the lowest dipole pass band as shown in Fig 4.1(a). The measured frequencies are fitted by fit by polynomials up to the third order. The deviation of the measured frequencies from those fitted are shown in Fig. 4.1(b) to check the smoothness of each disk frequency. Even if these remains an order of +-1MHz level residual errors from smooth curve, this value is much smaller than the required sigma

of 3MHz. The population of the deviation are shown in statistical histogram plot in Fig. 4.2. The standard deviation of the scattering is around 0.5MHz much less that the requirements.

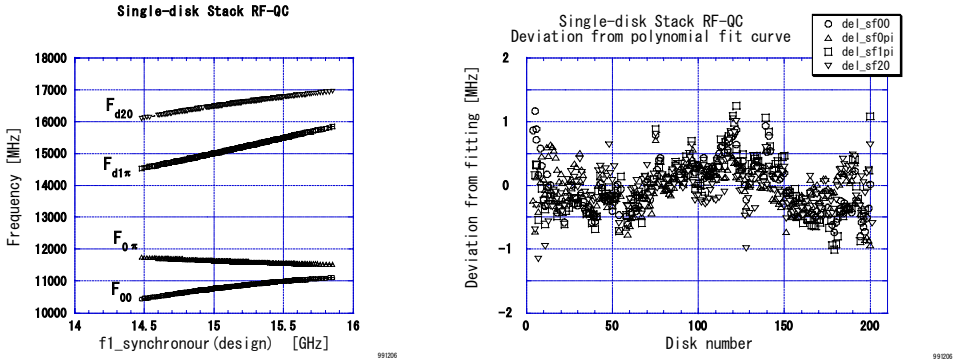

(a) (b)

Fig. 4.1 (a) Frequencies measured in single-disk set up as functions of synchronous frequency of lowest dipole pass band. (b) Frequency deviation from smooth curve obtained by fitting of measured frequencies as functions of design synchronous frequency.

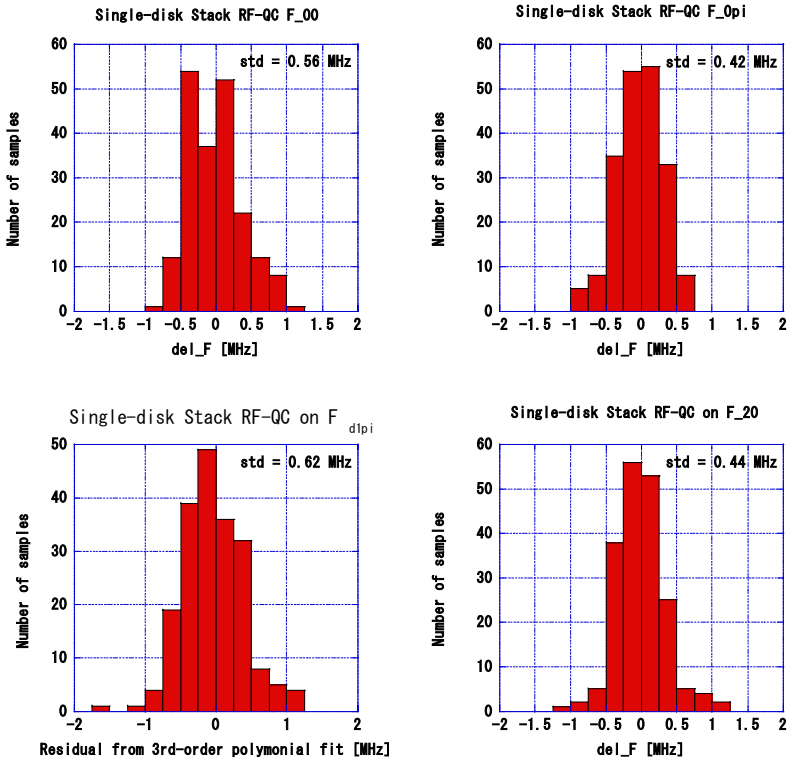

Fig. 4.2 Population of frequency deviations from smooth curves for four modes shown in Fig. 4.1(b).

There remains some systematic variation along the structure of 0.5MHz level. This is less than the roughly estimated tolerance of systematic error of the higher modes are of the order of a few MHz level. However, the deviation of frequencies from the design value should be carefully evaluated to confirm the structure to be within the requirement instead of sonly comparing to the smooth curves.

In Fig. 4.3 are shown the deviation of the measured frequencies from the design values in a very simple assumption to compare. The accelerating mode frequencies are calculated to be weighted average of F_{00} and $F_{0\pi}$ mode, while the lowest dipole synchronous mode is simply represented by the Fd1π mode to see the smoothness in a rather direct way than Fig. 4.1(b).

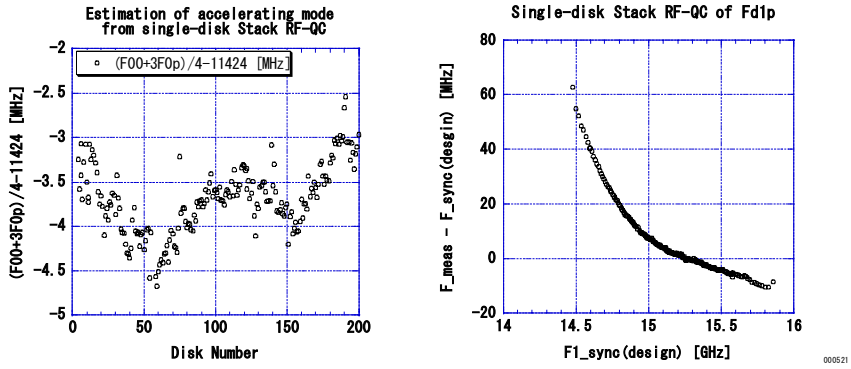

(a) (b)

Fig. 4.3 Frequency difference (a) between nominal accelerating mode frequency, 11.424GHz and that estimated from measured zero and π mode frequencies, (b) between lowest dipole mode frequencies, one from measured π mode and another from design synchronous mode.

4.2 Six-disk RF QC (accelerating mode)

Disk fabrication is done from the smaller numbered disk to larger by skipping the vacuum pumping disks. The accelerating mode frequency was evaluated from 3-disk and 6-disk measurements. Average frequency of each six-disk set up is shown in Fig. 4.3. The associated phase slip along the structure integrated from the front-end side is calculated and the feed forward values for "2b" in the later fabrication disks were applied as shown in the figure. Finally 16 vacuum pumping disks and several recovery disks were made.

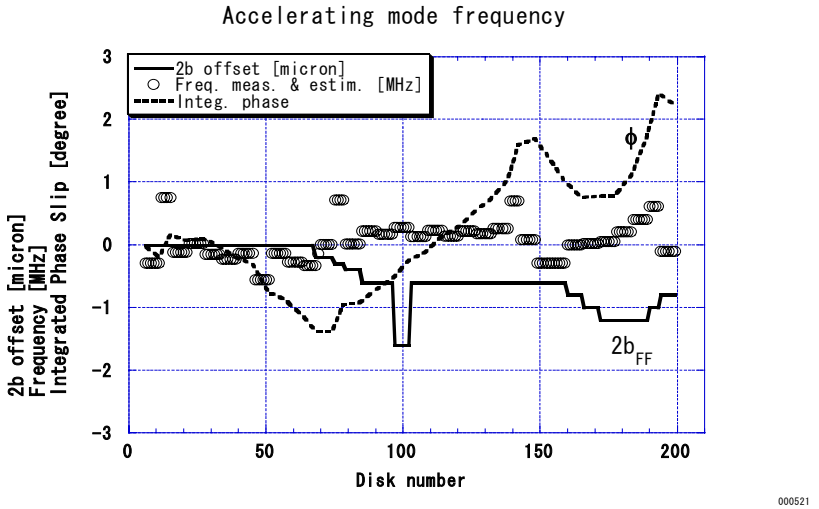

Fig. 4.4 Accelerating mode frequencies of each six consecutive disks (circles) and feed forward values on "2b"(solid line). Associated phase slip along the structure is also plotted in a dashed line.

In Fig. 4.5 shows the frequency difference between 6-disk set up and 3-disk set up. It measures the amount of frequency perturbation of probes on accelerating mode. It was found that the smooth increase of perturbation from input side to the output side by 50% is consistent to the estimation by the E and H field calculated by MAFIA. However, the peculiar behaviour appears in the vacuum pumping disks. They showed somewhat constant dependence on disk number but with much larger perturbation. The difference of these disks from the other standard ones are in their thin channel (2mmX5mm) for vacuum connecting between two HOM manifolds and the outside. The rough machining of these disks including 3D shapee cutting were performed by a different company than that for the other standard disks though we cannot detect any measurable difference in 3D shape between the disks supplied by the different companies. We do not now the mechanism yet.

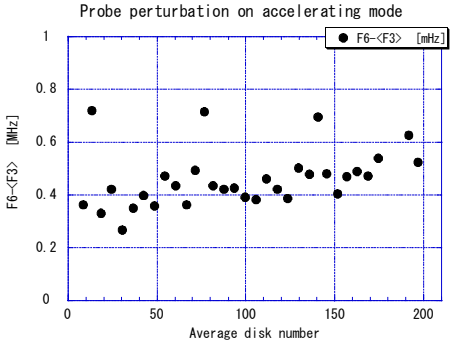

Fig. 4.5 Frequency difference between 6-disk set up and 3-disk set up.

4.3 Pseudo dispersion curves of six-disk set up (higher mode and manifold mode)

Transmission spectra, S_{12} versus frequency, in relevant frequency regions were taken for every 6-disk set up. Typical spectrum is shown in Fig. 4.6(a). As seen in the figure, four pass bands are evaluated from this spectrum. Three pass bands are bunched in a limited frequency region, the monopole pass band including the accelerating mode, the lowest dipole band and the second dipole band. The manifold pass band are spread in a wide frequency range. These classified mode frequencies are plotted in a dispersion diagram in Fig. 4.6(b). The coupling between dipole mode and manifold is clearly seen in the figure. The dispersion curves thus obtained are plotted for all of the six-disk set ups as shown in Fig. 4.7. The equivalent circuit results on these dispersions are compared to the experimental values to confirm the parametrization of the circuit model.

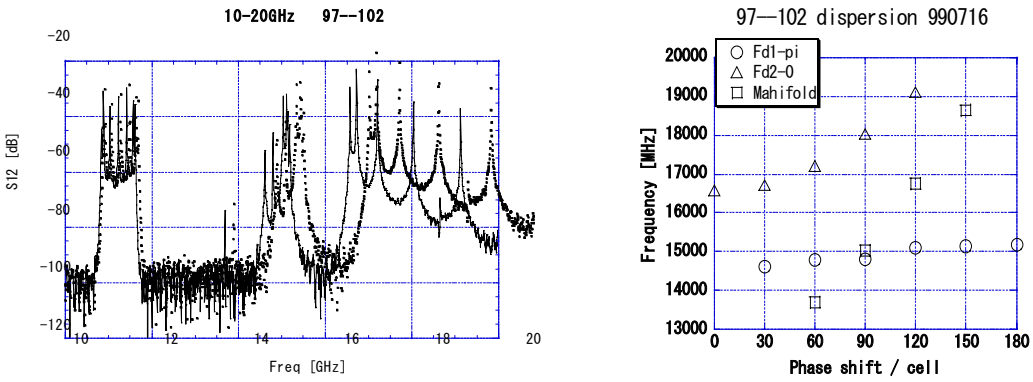

Fig. 4.6 (a) Spectrum of S12 in six-disk set up. (b) Resultant dispersion curve.

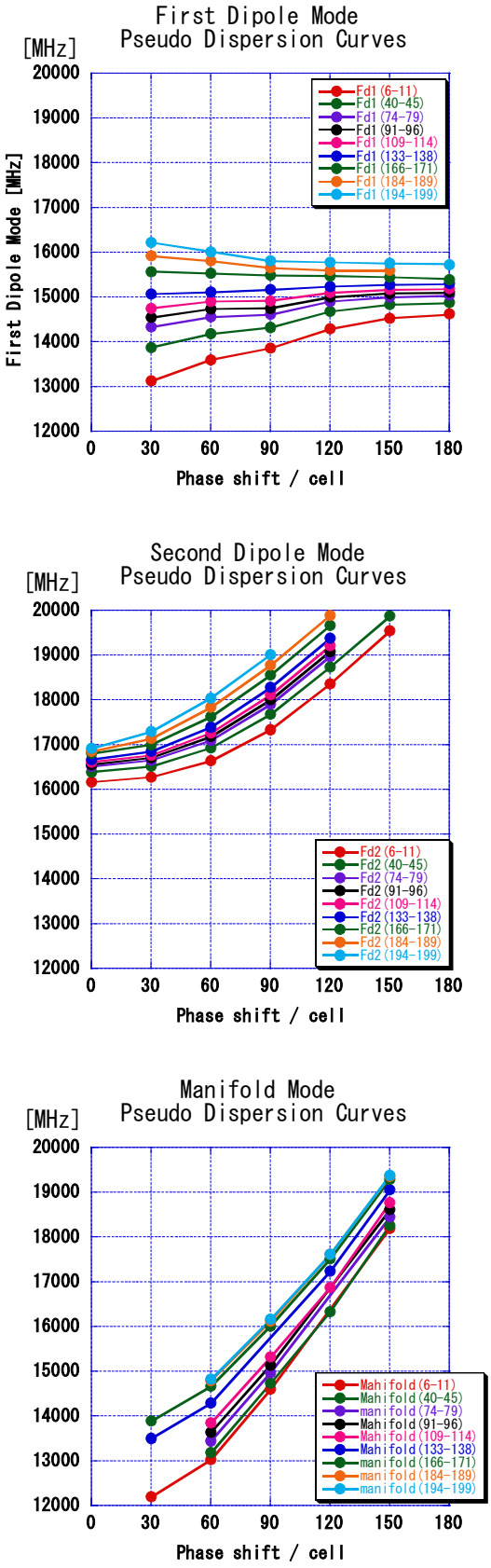

Fig. 4.7 Dispersion curves of all 6-disk measurement.

4.4 Measurement of special disks (near front end and output end)

The disks for the measurement shown in section 4.4 are all separated at the center of each accelerating cell so that it is symmetric and its cell radii at both sides are the same each other and they are designed to make the accelerating mode frequency right for the combination with the beam hole shape. Therefore, the pseudo $2\pi/3$ mode can easily be formed by simply shorting each end plane with a flat plate. However, some of disks in the front end and output end are separated at some other positions than the center of a cell. Therefore, the cell diameter was designed by averaging the effective cell diameters determined by the beam hole radii at both sides of the end cell. Therefore, the diameters of the dummy cells to short the stacked disks are to be determined to realize the pseudo $2\pi/3$ mode by cancelling the correction applied to the cell diameter of the end cell as the effect from the beam hole shape of the next disk which is not the disk to be measured.

In Fig. 4.8 is shown the measured S_{12} in six-disk set ups of front end and output end. By carefully designing the end cell and dummy half cells flowed the consideration stated in the previous paragraph, the frequency of the pseudo $2\pi/3$ mode can be evaluated.

Actually in RDDS1, we made a mistake that the diameter of the end cell (#203) was determined as the same as the actual design so that the averaging effect makes the radius 86 microns larger than the value inherent to the end disk itself. This made the measured frequencies deviate from the nominal one by 17MHz in six-disk set up and 34MHz in three-disk set up, which agreed with experimental values within 1 MHz. From this comparison, we confirmed that the fabricated disks near both ends are also good in precision.

The lowest dipole pass band appears in the frond end set up, while does not in the output end set up. This is due to the feature that the cell-to-cell coupling in the output end is too small comparing to the frequency spacing so that the dipole power cannot transmit to the other end, while it is large enough to communicate between cells in the front end. This cell-to-cell coupling effect plays an important role since there disks are not equipped with a coupling to the manifold.

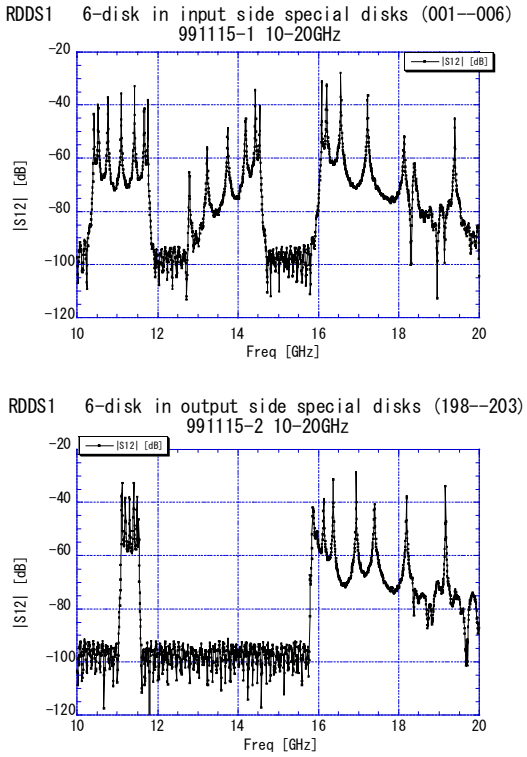

Fig. 4.8 Transmission spectrum of six disks.
(a) In input side, #1-6 and (b) output side, #199-203.

5. Summary and discussions

By sandwiching each disk with two flat plates, the smoothness of the frequencies of all of the disks along the structure was proved to be within 0.6 MHz rms. The three and six consecutive disks were stacked and also sandwiched by the same set up to evaluate the accelerating mode frequency with a precision of about 0.2MHz. The measurement on the previously made disks were feed-forwarded to the later fabrication of disks to make the integrated phase advance over the structure less than 5 degrees. This value is much smaller than 0.1MHz in average frequency and this tolerance cannot be met with any direct control of dimensions.

This method was proved to work for the fabrication of structure in a moderate speed to make a structure in a month or two. In order to develop a quality checking system for much higher production speed should be studied in future.

One of the trial in this direction, a choke set up (floating set up), was made where each disk was set on a choke stand with a finite gap and covered by the same choke set up on top again with a finite gap. The measured frequencies showed non-smooth behaviour for some of the cells. It seems to be related to the 3D geometry which intersects with the choke structure. The realization of the floating is one of the study items in near future.

Possible improvements in measuring set up

There found several items for the experimental set up to be improved in future.

1. Higher frequency measurement capability higher than 20GHz

It is better to measure dipole higher modes higher than the second to confirm the detuning of those modes. The limitation up to 20GHz was due to the limitation of the present network analyser.

2. Easy handling

The space for the operator to set the disks on the stack QC set up was not large enough because the space is just large enough to handle but not for easy handling. This makes the handling time long so that the possibility to acquire dusts increases and also the temperature of disk increases. We can easily design the set up by using wider V-block and remove pressure bars outer-wards, far from the operator's hands. In addition, the operator needs to look into the set up from almost above the set up, because one need to look carefully the narrow configuration especially for keeping the rotational alignment right. Such a situation for the operator to look over the set up should be avoided to reduce the dusts on the mating surfaces.

3. Better cleanness

The present set up is located 1.2m above floor level to make the set up less influenced by the dusts flung up while people walk around. It is good but the set up should be modified as described in the paragraph above so that the high-level set up becomes effective where the direct air flow from HEPA filter blows the set up with few dirty things and for less period around the flow.

4. Lower contact pressure

We did not understand well about the deterioration of the mating surfaces after many times pressurization. Even if we care about dusts much, we observed increasing number of scratches and marks due to some string-like object. Many times we can recognize the same pattern in the opposite side of the mating plane. Such inclusion of dusty material should be minimized by taking care of clean operation.

We should also check the possibility of deterioration due to metal-to-metal contact at high pressure. If the deterioration speed decreases by reducing the pressure, it should be reduced down to the value slightly above the saturation level.

Acknowledgments

The authors greatly acknowledge Prof. D. Burke of SLAC and Profs. M. Kihara and K. Takata of KEK for keeping active the collaboration program which this study is based on.

The authors want to thank Dr. I. Mejuev of PFU Co. Ltd. and Mr. E. Kadokura of KEK for making the control program to measure with a network analyser and record the data for the later use.

References

[1] NLC/JLC group, "International Study Group Progress Report", SLAC R-559 and KEK Report 2000-7, April, 2000.
[2] Zeroth-Order Design Report for the Next Linear Collider, SLAC Report-474, 1996.
[3] JLC Design Study, KEK Report 97-1, 1997.
[4] Y. Higashi et al., KEK-Report 2000-1, May 2000.
[5] J. Wang et al., Proceedings of Linear Accelerator Conference, LINAC2000, TUA03, Monterey, 2000.
[6] Z. Li et al., Proceedings of the 1999 Particle Accelerator Conference, PAC99, FRA41, New York, 1999.
[7] N. Hitomi et al., Proceedings of Linear Accelerator Conference, LINAC2000, TUA01, Monterey, 2000.
[8] T. Higo et al., Proceedings of Linear Accelerator Conference, LINAC2000, TUA02, Monterey, 2000.